Dual broadband infrared absorptance enhanced by magnetic polaritons using graphene-covered compound metal gratings

NGHIA NGUYEN-HUU,[1,2,3,*] **JAROMIR PISTORA,**[4] **AND MICHAEL CADA**[2]

[1]*Nanotechnology Centre, VSB - Technical University of Ostrava, Ostrava-Poruba 708 33, Czech Republic*
[2]*Department of Electrical and Computer Engineering, Dalhousie University Halifax, Nova Scotia B3J 2X4, Canada*
[3]*LED Roadway Lighting Ltd., 115 Chain Lake Drive Halifax, Nova Scotia B3S1B3, Canada*
[4]*Regional Materials Science and Technology Centre, Faculty of Material Technologies, VSB -Technical University of Ostrava, Ostrava-Poruba 708 33, Czech Republic*
*nghianano@gmail.com

Abstract: A dual broadband perfect absorber based on a graphene-covered compound silver (Ag) grating structure working in the infrared (0.8–2.1 μm) regime is proposed and investigated numerically. Two distinct absorption peaks approximately 1.0 are achieved by the excitation of magnetic polaritons over a large range of incident angles from 0 to 70 degrees. The physics underlying the structure is also explained by computing interactions of electromagnetic fields with the graphene and the Ag grating. In addition, it has shown that the absorption peaks can be tuned by changing geometric parameters of the structure; however, their spectral shape and absorption remain unchanged. Furthermore, the proposed compound grating with a graphene overlay provides potential applications for infrared absorbing devices.

1. Introduction

Light enhancement in plasmonic nanostructures has attracted a great attention form the research community since it provides tremendous applications for solar cells, photodetectors, sensors, nanoimaging devices, thermal emitters, and metamaterial absorbers [1–12]. The enhancement was theoretically and experimentally demonstrated due to such phenomena of surface plasmon polaritons, magnetic polaritons, Fano resonance, or cavity resonance [13–23]. Recently, various single-frequency perfect absorbers working in gigahertz, terahertz, and infrared (IR) ranges have been actively investigated due to their various applications such as IR detectors, bio/chemical sensing, IR imaging devices, thermo bolometers, and so forth [24–32]. To be detailed, IR perfect absorbers were constructed based on one dimensional (1D) or 2D multiple layered structures comprising a top metamaterial layer, a middle dielectric spacer layer, and a bottom metal reflector or silicon substrate [15–17,23,31]. In addition to that, absorbers based on grating structures consisting of a graphene layer covering a metal/dielectric/metal or metal grating have also been studied physically [19–21,23,33]. The enhanced absorption was caused by various resonances occurring either in the top metal, in the spacer, or coupling each other. Although many IR absorbers were proposed numerically and experimentally, their narrowly spectral bandwidths limited the potential applications of single-band absorbers.

To address the narrow bandwidth problem, absorbers featuring dual and multiband absorption in the IR regime have been proposed with different geometric shapes [34–37]. For instance, these absorbers were designed by tuning their geometric dimensions in a single, multiple unit cells, or vertically stacked multiple layers [36,38]. Dual-band absorbers were also constructed based on 1D or 2D multiple hole structures with a graphene overlay

[18,34,35]. Similarly, an absorber was built based on two different dielectric spacer materials or by changing different thicknesses of the dielectric material in a single unit cell [34,37]. Although the previous designed IR absorbers have provided very high absorption efficiency, they owned complex geometric structures which were not feasible to be manufactured and worked in a narrow range of wavelengths as well. Therefore, it is necessary to design multiple band perfect absorbers featuring an easily-fabricated geometry and near unity absorption. Subwavelength grating structures whose dimensions are smaller comparable with incident light are playing a vital key in fulfilling the requirement of high efficient devices, which could be used to build multiple band perfect absorbers.

Most recently, the subwavelength structures combined with a graphene overlay have shown that the absorption enhancement is greatly enhanced, and they could work as single-frequency absorbers in the IR region [22,39]. However, compound gratings (CG) covered by a graphene sheet used to enhance dual band IR absorption has not been addressed yet. Accordingly, in this paper we design and investigate a dual band perfect absorber in the near IR range based on graphene-covered CGs. A CG has a period including multiple nonidentical grating periods [40], and it was also known as a double-period grating, a dual-pitch grating, a dual-period grating, and a complex grating [41–43]. On the contrary, a simple grating (SG) features a single period [3]. In the present study the absorber exhibits two distinct absorption peaks with approximately unity absorptance and is insensitive to a large range of incident angles. The physical phenomenon to enhance the absorptance is also studied. Furthermore, the resonant wavelength of the two bands can be tailored by varying the geometry of the graphene-covered CG structure. Generally, the dual band perfect absorber is proposed in the present study using a compound metallic grating with a graphene overlay that provides practical uses of enhancing absorption to be nearly perfect.

2. Theoretical description

Figure 1 shows the schematic illustration of a double layered compound grating (DLCG) structure made of silver (Ag). The geometry of the DLCG structure is depicted by the period (Λ), the grating thickness d_1 and the lamella width $f_{v1}\Lambda$ (f_{v1} is the filling ratio, $0 < f_{v1} < 1$) of the SG layer, and the grating thickness d_2, the lamella width $f_{v2}\Lambda$ (f_{v2} is the filling ratio, $0 < f_{v2} < 1$) and the lamella width $f\Lambda$ (f is the filling ratio, $0 < f < 1$) of the CG layer. The incident light including transverse magnetic (TM) **H** or transverse electric waves (TE) **E** travels through a free space with an orientation defined by the polar angle θ between the wavevector **k** and the surface normal **z**. Note that **H** and **E** denote oscillation directions of magnetic and electric fields, respectively.

For the one-dimensional grating shown in Fig. 1, the electromagnetic field is independent to *y*-axis because the wavevectors of all diffracted waves lie in the *x-z* plane, and thus, there are no excitations in the *y* direction. In this study, the TM wave is used for analyses because as demonstrated surface plasmon polaritons and magnetic polaritons could only be excited when the magnetic field is in the *y* direction. These resonances are solely or altogether coupled resulting in enhancing the absorption of structures [22–24,28,29]. The Ag base below the grating is assumed to be thick enough as an opaque, and accordingly, the transmittance is equal to 0, and the absorptance (α) can be computed from one minus the reflectance (R), $\alpha = 1 - R$, where the reflectance was calculated by the rigorous coupled-wave analysis (RCWA) based on MatLab programming [30]. The results obtained from the RCWA and Comsol Multiphysics were validated with those in the previous papers [23,28]. It has demonstrated that simple deep gratings significantly enhance the absorptance of graphene [22,23], and thus, this manuscript firstly represents an optimization of the high absorptance of SG and CG structures, and based on that the constructed graphene-covered CG structures are then proposed with dual band absorptance nearly unity in a wavelength range between 0.8 and 2.1 μm.

In our calculation, the optical property of Ag is caomputed using a Lorenzt-Drude model [44,45] while the dielectric function of graphene is described as $\varepsilon(\omega) = 1 + i\sigma_s / (\varepsilon_0 \omega \delta)$ [46] where σ_s, ε_0, and ω are the sheet conductance, the vacuum permittivity, and the angular frequency, respectively. The sheet conductance σ_s ($\sigma_s = \sigma_D + \sigma_I$) including the contribution of a Drude (intraband) term σ_D and an interband term σ_I is described theoretically and experimentally in [47]. Based on the intraband and interband expressions [47], the parameters are used for the calculation such as the chemical potential ($\mu = 0.3$ eV), relaxation time ($\tau = 10^{-13}$ s), the temperature $T = 300$K, and the graphene thickness $\sigma = 0.3$ nm. It is noted that with the condition of $kBT \ll \mu$, the graphene conductance is constant ($\sigma s = \sigma I = e2/4\hbar$) in the visible and IR region [47]. Note that the properties of Ag are calculated based on the Lorenzt Drude model that was constructed by Rakic *et al.* [45]. There are some reasons using this model. Firstly, the parameters of the Lorentz-Drude function were fitted in a large range of energy from 0.125 eV (or wavelength of 12.4 μm) to 6 eV (or wavelength of 0.2 μm), and the data was tabulated based on experimental work of four research groups [48] and was also published in [49]. Secondly, the function used for modeling the optical properties of 11 metals was a flexible and convenient selection for simulations and optimizations. Lastly, the data was validated for its consistency of the optical constants based on calculations of a relaxation time [50]. The result has shown that its relaxation time was constant in the free electron region while other data displayed an unstable trend [50-52].
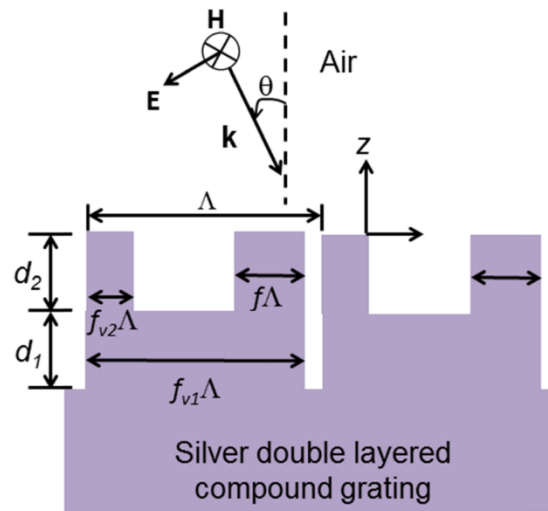

Fig. 1. Schematic illustration of the double layered compound Ag grating (DLCG). Their geometries are defined by the grating period Λ, the grating thicknesses d_1 and d_2, and the lamella widths $f_{v1}\Lambda$, $f_{v2}\Lambda$, and $f\Lambda$ (f_{v1} is varied filling ratio of SG, f_{v2} and f are varied and fixed filling ratios of CG, respectively). The transverse magnetic wave (**H**) (parallel to the grating grooves or y-axis) is incident on the grating with a wavevector **k** and an angle θ

3. Results and discussion

To optimize a CG absorber, we first simulated a SG structure comprising an Ag grating on top of an Ag substrate with a fixed grating period ($\Lambda = 400$ nm) and a fixed thickness ($d_1 = 200$ nm) as a function of wavelength λ and the filling ratio f_{v1}. Then, we calculated the SG structure with the same d_1 of 200 nm and the filling ratio to be found with a high absorptance ($f_{v1} = 0.95$) as a function of wavelength λ and grating period Λ. Finally, we simulated the SG with the fixed parameters including $\Lambda = 400$ nm and $f_{v1} = 0.95$ as a function of wavelength λ and grating thickness d_1. Results have shown that the SG featuring the property of a deep grating with the filling ratio of 0.95 exhibits high absorptance in a wavelength range from 1.6

to 1.8 μm when the parameter of Λ and d_1 are fixed. The result was also agreed with previous study on deep metal SG structures [22,23]. When the period of the deep grating was varied from 200 nm to 800 nm, the absorptance spectrum shifted from the wavelength of 2.1 μm to 1.5 μm. Similarly, when the grating thickness was changed from 50 nm to 800 nm, the high absorption was obtained with different thickness d_1. For example, a single-frequency absorber with a high absorptance at a peak wavelength of 1.1 μm or 1.6 μm could be created with a thickness of 400 nm or 600 nm, respectively.

Finally, from the obtained results a single SG could not offer a dual bandwidth and maximum absorption although it was able to offer a high absorption based on the characteristics of a deep grating. Accordingly, a single CG on top of an Ag substrate consisting of two lamellae with different filling ratios (f_{v2} and f), the grating period of 400 nm, and the grating thickness d_2 of 200 nm was investigated. Interestingly, the maximum absorptance of the CG was achieved in a wide range of f_{v2} from 0.05 up to 0.50. Note that the single CG grating to be simulated in the present study includes two grating periods with a fixed lamella of 180 nm ($f = 0.45$) and another is varied (varied f_{v2}) with a condition satisfied to be a deep grating. From the optimized results of the SG and CG structures, it can be concluded that the double layered compound grating made of a single SG and a single CG on top of an Ag substrate was suitably selected for the design of dual bandwidth perfect absorbers.
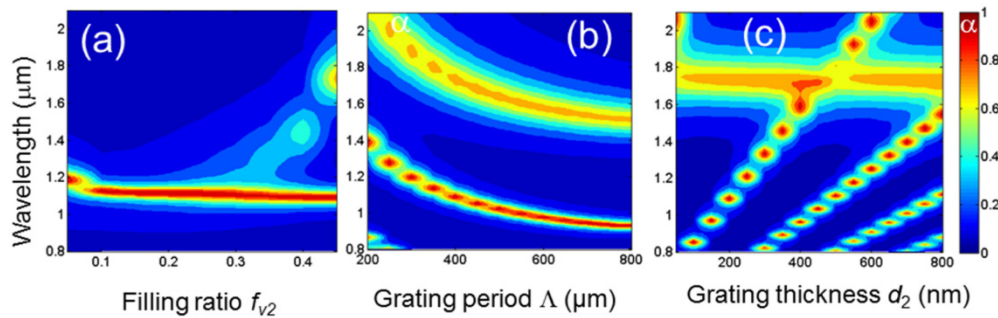

Fig. 2. Absorptance (α) contours for TM waves at normal incidence for the double layered compound Ag grating (a) with the fixed parameters including $\Lambda = 400$ nm, $d_1 = 200$ nm, and $f_{v1} = 0.95$ as a function of wavelength λ and f_{v2}, (b) with the fixed parameters includes $d_1 = 200$ nm, $d_2 = 200$ nm, $f_{v1} = 0.95$, and $f_{v2} = 0.45$ as a function of wavelength λ and grating period Λ, (c) with the fixed parameters includes $\Lambda = 400$ nm, $d_1 = 200$ nm, $f_{v1} = 0.95$, and $f_{v2} = 0.45$ as a function of wavelength λ and grating thickness d_2

Figure 2(a) exhibits the absorptance for TM waves at $\theta = 0°$ of the DLCG with the fixed parameters including $\Lambda = 400$ nm, $d_1 = d_2 = 200$ nm, and $f_{v1} = 0.95$ as a function of the wavelength λ and the filling ratio f_{v2}. It is noted that the parameters such as $\Lambda = 400$ nm, $d_1 = 200$ nm, and $f_{v1} = 0.95$ of the SG are fixed since the optimal absorptance is found to be maximum as analyzed above. From Fig. 2(a), it can be seen that the normal absorptance of the DLCG is obtained with a maximum value in a wide range of the filling ratio from 0.1 to 0.45; however, at $f_{v2} = 0.45$ they are two distinct peaks appearing at wavelengths of around 1.17 μm and 1.7 μm. The filling ratio, $f_{v2} = 0.45$, is the maximum value in a range of 0 and 0.45 to be optimized for the DLCG, and the DLCG becomes a double layered simple grating (DLSG) structure when f_{v2} is greater than 0.45 (the DLSG is not objective of this study).

For the purpose of designing dual band perfect absorbers, from the result computed in Fig. 2(a) the DLCG with $\Lambda = 400$ nm, $d_1 = 200$ nm, $d_2 = 200$ nm, $f_{v1} = 0.95$, and optimal $f_{v2} = 0.45$ was selected for a detailed investigation since it exhibited dual band absorptance. Figure 2(b) illustrates the absorptance (α) contours of the DLCG for TM waves at normal incidence with the fixed parameters includes $d_1 = 200$ nm, $d_2 = 200$ nm, $f_{v1} = 0.95$, and $f_{v2} = 0.45$ as a function of wavelength λ and grating period Λ. It can be seen that when the grating period

increases from 200 nm to 800 nm, the dual absorptance peak of the DLCG shifts to short wavelengths. Meanwhile, Fig. 2(c) shows the normal absorptance of the DLCG with the fixed parameters includes Λ = 400 nm, d_1 = 200 nm, f_{v1} = 0.95, and f_{v2} = 0.45 as a function of wavelength λ and grating thickness d_2. The feature of the absorptance spectrum shown in Fig. 2(c) has two bands while there is only one band of a SG structure (not shown here); accordingly, with different grating thickness the absorber-based the CG could display a dual band absorptance spectrum in a short and long wavelength range. Therefore, the optimal parameters of the DLCG including Λ = 400 nm, $d_1 = d_2$ = 200 nm, f_{v1} = 0.95, and f_{v2} = 0.45 were selected since the DLCG provided a dual band perfect absorptance working in the near IR regime.
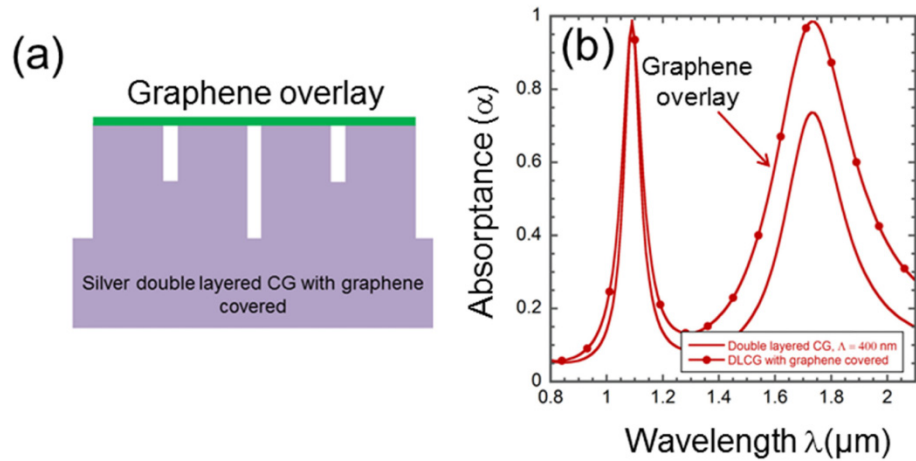

Fig. 3. (a) Schematic illustration of the designed DLCG structure featuring geometric parameters as same as those in Fig. 1 with a graphene overlay; and (b) Normal absorptance spectrum of the DLCG with and without a graphene overlay

Figure 3 displays the proposed DLCG with the grating period (Λ = 400 nm), the grating thicknesses of the SG and CG layers ($d_1 = d_2$ = 200 nm), and the filling ratios f_{v1} = 0.95, and f_{v2} = 0.45 with a graphene overlay having a thickness of 0.3 nm. Figure 3(b) illustrates the absorptance spectrum for TM waves at θ = 0° with two resonances, MP1 at λ_{MP1} = 1.73 μm and MP2 at λ_{MP2} = 1.09 μm corresponding the fundamental mode and the second harmonic of magnetic polaritons, respectively. The higher order of MP is, the peak absorption increases [19]. It is revealed that the absorptance peaks at λ_{MP2} = 1.09 μm and λ_{MP1} = 1.73 μm in Fig. 3(b) are enhanced up to a maximum value of 1.0 when the DLCG is covered by a graphene sheet. Interestingly, absorptance spectra of the DLCG to be simulated with different grating periods (e.g., Λ = 600 nm and 800 nm) and fixed other grating parameters showed that they similarly feature two modes of MPs and their spectral bandwidths remain unchanged although the peaks shift to shorter wavelengths (the results were not shown here).

Figure 4 shows the absorptance contours of the DLCG and graphene-covered DLCG structures as a function of wavelength λ and angle of incidence θ. It can be seen from Figs. 4(a) and 4(b) that the absorptance at the short-wavelength peaks (λ_{MP2} = 1.09 μm) of the two grating structures is found to be approximately maximum in a wide range of incident angles from 0 to 60°. On the contrary, the absorptance of the CG at the long-wavelength peak (λ_{MP1} = 1.73 μm) shown in Fig. 4(a) is not high in a narrow range of incident angles while that of the graphene-covered DLCG shown in Fig. 4(b) is obtained to be near unity to 50° and decreases to 0.7 to 70°. Generally, with a graphene overlay, the absorptance at dual peaks of the DLCG increases to the maximum value of 1.0 and is insensitive to a wide range of angles of incidence.
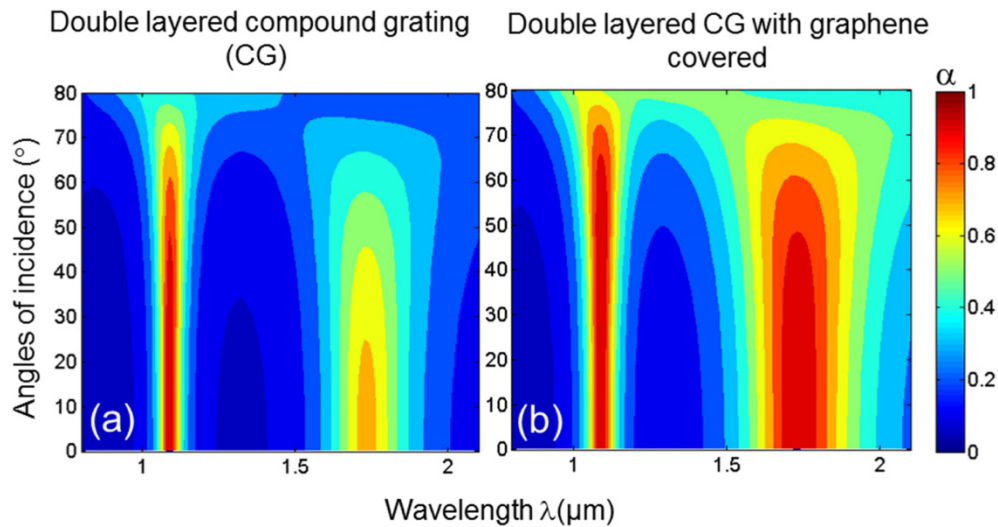
Fig. 4. Absorptance contours of (a) the DLCG and (b) graphene-covered DLCG as a function of the wavelength and angles of incidence

To manufacture the proposed DLCG structure with such geometries, one could firstly fabricate graphene using chemical vapor deposition on a copper foil and secondly etch the deep trench (groove) grating structures based on a cryogenic etching method [53–55]. To be detailed, the fabrication process starts by pattering grating lines on a polymer resist layer on an Ag substrate using nanoimprint and then using chromium shadowing and reactive ion etching (RIE) to etch the resist layer to form an etch mask. Continually, deep trenches of the gratings are created by the cryogenic RIE, and the mask materials are fianally removed by a plasma cleaning process. Previous studies have demonstrated that this cost-efficient manufacturing method was successfully implemented to create deep trenches with a deep width to wall thickness ratio (aspect ratio) up to 40 [53] and a deep trench width of 20 nm with an aspect ratio of 8 [54].

Figures 5(a)-(f) describe the magnetic and electric field distributions at the resonance wavelengths of magnetic polaritons (λ_{MP2} = 1.09 μm, λ_{MP1} = 1.73 μm at θ = 0°) for the DLCG with and without a graphene overlay. In Figs. 5(a), 5(b), 5(d), and 5(e), the color contour represents the magnetic field and the arrows indicate normalized electric fields. Figures 5(c) and 5(f) show the normalized magnitude of electric field of the DLCG at λ_{MP1} = 1.73 μm and θ = 0° while the insert figures display the magnified electric field at the opening of the grating trenches. It is seen from Figs. 5(a), 5(b), 5(d), and 5(e) that the strong magnetic field traps inside the trenches (grating grooves) of both structures with and without graphene overlay; however, the magnetic field occupies in the longer trench stronger than that in the short trench. In addition to that, the magnetic fields at λ_{MP2} = 1.09 μm trapping in the trench much more than that at λ_{MP1} = 1.73 μm; this results a higher absorptance at the higher order MP as seen in Figs. 3 and 4.

As an illustration shown in Figs. 5(c) and 5(f), the electric field similarly traps inside the trenches of the both grating structures. It can be seen that the electric field shown in Fig. 5(c) traps more inside the trench of the DLCG without a graphene overlay while that of the DLCG covered by a graphene sheet shown in Fig. 5(f) concentrates less. However, taking a close look at the graphene overlay on the grating opening as seen in the insert figure of Fig. 5(f), one can see the electric field ocsilateing stronger at the interface. As a result, this makes graphene absorbing more energy that is also well-agreed with demonstrations in the previous studies [22,39].
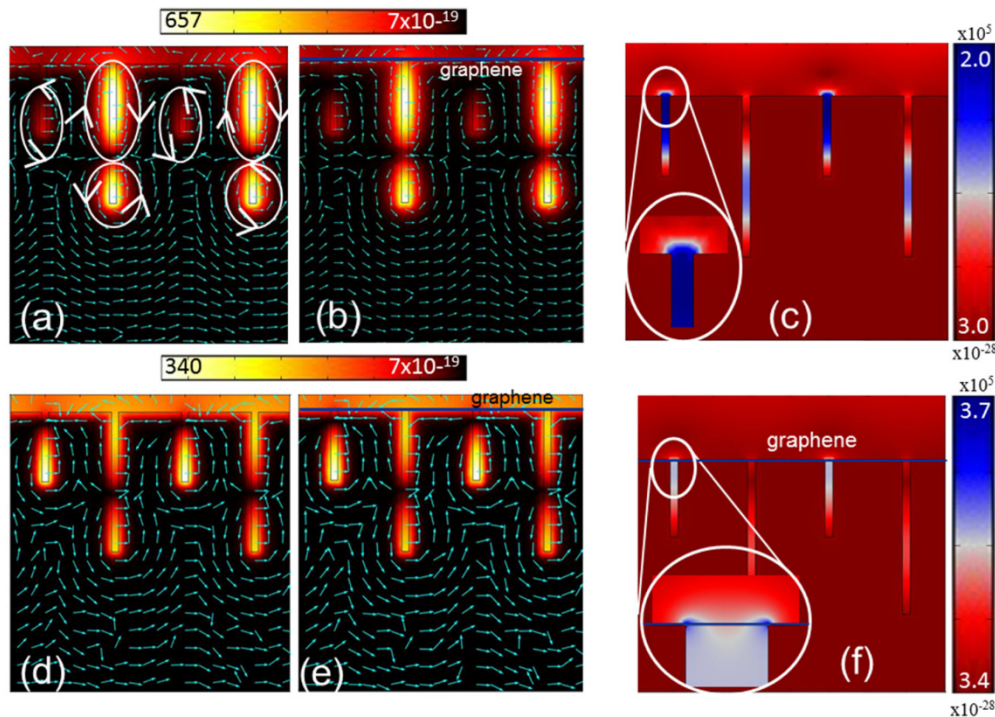
Fig. 5. Electromagnetic fields for DLCG structures for TM waves at normal incidence: (a) and (b) the DLCG with and w/o graphene at the peak λ_{MP2} = 1.09; (d) and (e) the DLCG with and w/o a graphene sheet at the peak λ_{MP1} = 1.73 μm; (c) and (f) the color indicates the normalized magnitude of the electric field of the DLCG with and w/o a graphene sheet at the resonance wavelength λ_1 = 1.73 μm. The color in Figs. (a), (b), (d), and (e) show normalized magnitude of the magnetic field, while the arrows indicate the normalized electric field. The insert figures in Figs. (c) and (f) show the enhancement of electric fields (blue spots) at the opening of the grating trench.

Generally, Figs. 5(a)-(e) reveal the magnetic polaritons (MPs) to be excited in the DLCG with and without a graphene layer. The MP is a strong coupling between a magnetic resonance inside grating structures and external electromagnetic waves. As shown in these figures, the time-varying magnetic field parallel to the *y* direction generates a closed current loop around the trenches in the structures where the strong localized magnetic field is created, and it then forms the MP (it is known as Lenz's law). In addition to that, there is no occurrence of surface plasmon polaritons based on the electromagnetic calculation shown in the above figures. Therefore, the enhancement of absorptance in the graphene-covered DLCG structures was caused by the magnetic polariton excitation with two modes of resonances.

4. Conclusion

The manuscript has presented the simple design of the novel plasmonic structure, namely the graphene-covered double layered compound Ag grating working as a dual band perfect absorber. Its absorptance was found to be 100% and its dual band spectrum was insensitive to a large range of incident angles from 0 to 70°. The physics behind the DLCG with the graphene overlay was demonstrated due to the excitation of the magnetic polaritons. Furthermore, the proposed structure feasible to be manufactured provides tremendous applications for designing multiple band perfect IR absorbers based on graphene-covered compound metallic gratings.

References

1. K. R. Catchpole and A. Polman, "Plasmonic solar cells," Opt. Express **16**(26), 21793–21800 (2008).
2. J. N. Munday and H. A. Atwater, "Large integrated absorption enhancement in plasmonic solar cells by combining metallic gratings and antireflection coatings," Nano Lett. **11**(6), 2195–2201 (2011).
3. N. Nguyen-Huu, M. Cada, and J. Pištora, "Investigation of optical absorptance of one-dimensionally periodic silicon gratings as solar absorbers for solar cells," Opt. Express **22**, A68–A79 (2014).
4. J. Hao, J. Wang, X. Liu, W. J. Padilla, L. Zhou, and M. Qiu, "High performance optical absorber based on a plasmonic metamaterial," Appl. Phys. Lett. **96**(25), 251104 (2010).
5. Z. Yu, G. Veronis, S. Fan, and M. L. Brongersma, "Design of midinfrared photodetectors enhanced by surface plasmons on grating structures," Appl. Phys. Lett. **89**(15), 151116 (2006).
6. J. Rosenberg, R. V. Shenoi, T. E. Vandervelde, S. Krishna, and O. Painter, "A multispectral and polarization-selective surface-plasmon resonant midinfrared detector," Appl. Phys. Lett. **95**(16), 161101 (2009).
7. N. Liu, M. Mesch, T. Weiss, M. Hentschel, and H. Giessen, "Infrared perfect absorber and its application as plasmonic sensor," Nano Lett. **10**(7), 2342–2348 (2010).
8. N. Nguyen-Huu, M. Cada, J. Pištora, and K. Yasumoto, "Tunable optical filter based on gold and silver double-sided gratings and its application as plasmonic sensor," J. Lightwave Technol. **32**(21), 3477–3484 (2014).
9. Y. Zhao, S.-C. S. Lin, A. A. Nawaz, B. Kiraly, Q. Hao, Y. Liu, and T. J. Huang, "Beam bending via plasmonic lenses," Opt. Express **18**(22), 23458–23465 (2010).
10. M. Diem, T. Koschny, and C. M. Soukoulis, "Wide-angle perfect absorber/thermal emitter in the terahertz regime," Phys. Rev. B Condens. Matter Mater. Phys. **79**(3), 033101 (2009).
11. N. Nguyen-Huu, Y.-B. Chen, and Y.-L. Lo, "Development of a polarization-insensitive thermophotovoltaic emitter with a binary grating," Opt. Express **20**(6), 5882–5890 (2012).
12. T.-J. Yen, W. J. Padilla, N. Fang, D. C. Vier, D. R. Smith, J. B. Pendry, D. N. Basov, and X. Zhang, "Terahertz magnetic response from artificial materials," Science **303**(5663), 1494–1496 (2004).
13. J. Chen, W. Fan, P. Mao, C. Tang, Y. Liu, Y. Yu, and L. Zhang, "Tailoring plasmon lifetime in suspended nanoantenna arrays for high-performance plasmon sensing," Plasmonics **12**(3), 529–534 (2017).
14. J. Chen, T. Zha, T. Zhang, C. Tang, Y. Yu, Y. Liu, and L. Zhang, "Enhanced magnetic fields at optical frequency by diffraction coupling of magnetic resonances in lifted metamaterials," J. Lightwave Technol. **35**(1), 71–74 (2017).
15. J. Chen, T. Zhang, C. Tang, P. Mao, Y. Liu, Y. Yu, and Z. Liu, "Optical magnetic field enhancement via coupling magnetic plasmons to optical cavity modes," IEEE Photonics Technol. Lett. **28**(14), 1529–1532 (2016).
16. J. Chen, C. Tang, P. Mao, C. Peng, D. Gao, Y. Yu, Q. Wang, and L. Zhang, "Surface-plasmon-polaritons-assisted enhanced magnetic response at optical frequencies in metamaterials," IEEE Photonics J. **8**(1), 1–7 (2016).
17. R. Feng, J. Qiu, Y. Cao, L. Liu, W. Ding, and L. Chen, "Wide-angle and polarization independent perfect absorber based on one-dimensional fabrication-tolerant stacked array," Opt. Express **23**(16), 21023–21031 (2015).
18. R. Feng, J. Qiu, L. Liu, W. Ding, and L. Chen, "Parallel LC circuit model for multi-band absorption and preliminary design of radiative cooling," Opt. Express **22**, A1713–A1724 (2014).
19. L. Wang and Z. Zhang, "Resonance transmission or absorption in deep gratings explained by magnetic polaritons," Appl. Phys. Lett. **95**(11), 111904 (2009).
20. B. Zhao and Z. M. Zhang, "Study of magnetic polaritons in deep gratings for thermal emission control," J. Quant. Spectrosc. Radiat. Transf. **135**, 81–89 (2014).
21. B. Zhao and Z. M. Zhang, "Strong plasmonic coupling between graphene ribbon array and metal gratings," ACS Photonics **2**(11), 1611–1618 (2015).
22. B. Zhao, J. Zhao, and Z. Zhang, "Enhancement of near-infrared absorption in graphene with metal gratings," Appl. Phys. Lett. **105**(3), 031905 (2014).
23. Q. Pan, J. Hong, G. Zhang, Y. Shuai, and H. Tan, "Graphene plasmonics for surface enhancement near-infrared absorptivity," Opt. Express **25**(14), 16400–16408 (2017).
24. Y. Q. Ye, Y. Jin, and S. He, "Omnidirectional, polarization-insensitive and broadband thin absorber in the terahertz regime," J. Opt. Soc. Am. B **27**(3), 498–504 (2010).
25. N. I. Landy, S. Sajuyigbe, J. J. Mock, D. R. Smith, and W. J. Padilla, "Perfect metamaterial absorber," Phys. Rev. Lett. **100**(20), 207402 (2008).

26. C.-M. Wang, Y.-C. Chang, M.-W. Tsai, Y.-H. Ye, C.-Y. Chen, Y.-W. Jiang, Y.-T. Chang, S.-C. Lee, and D. P. Tsai, "Reflection and emission properties of an infrared emitter," Opt. Express **15**(22), 14673–14678 (2007).
27. J. Wang, Y. Chen, J. Hao, M. Yan, and M. Qiu, "Shape-dependent absorption characteristics of three-layered metamaterial absorbers at near-infrared," J. Appl. Phys. **109**(7), 074510 (2011).
28. T. Maier and H. Brückl, "Wavelength-tunable microbolometers with metamaterial absorbers," Opt. Lett. **34**(19), 3012–3014 (2009).
29. Z. Song, M. Wei, Z. Wang, G. Cai, Y. Liu, and Y. Zhou, "Terahertz absorber with reconfigurable bandwidth based on isotropic vanadium dioxide metasurfaces," IEEE Photonics J. **11**(2), 1–7 (2019).
30. Z. Song, Z. Wang, and M. Wei, "Broadband tunable absorber for terahertz waves based on isotropic silicon metasurfaces," Mater. Lett. **234**, 138–141 (2019).
31. M. Wei, Z. Song, Y. Deng, Y. Liu, and Q. Chen, "Large-angle mid-infrared absorption switch enabled by polarization-independent GST metasurfaces," Mater. Lett. **236**, 350–353 (2019).
32. J. Chen, W. Fan, T. Zhang, C. Tang, X. Chen, J. Wu, D. Li, and Y. Yu, "Engineering the magnetic plasmon resonances of metamaterials for high-quality sensing," Opt. Express **25**(4), 3675–3681 (2017).
33. T. Sang, J. Gao, X. Yin, H. Qi, L. Wang, and H. Jiao, "Angle-insensitive broadband absorption enhancement of graphene using a multi-grooved metasurface," Nanoscale Res. Lett. **14**(1), 105 (2019).
34. N. Zhang, P. Zhou, D. Cheng, X. Weng, J. Xie, and L. Deng, "Dual-band absorption of mid-infrared metamaterial absorber based on distinct dielectric spacing layers," Opt. Lett. **38**(7), 1125–1127 (2013).
35. B. Liu, C. Tang, J. Chen, Q. Wang, M. Pei, and H. Tang, "Dual-band light absorption enhancement of monolayer graphene from surface plasmon polaritons and magnetic dipole resonances in metamaterials," Opt. Express **25**(10), 12061–12068 (2017).
36. H. Lee and J. Wu, "A wide-angle dual-band infrared perfect absorber based on metal–dielectric–metal split square-ring and square array," J. Phys. D Appl. Phys. **45**(20), 205101 (2012).
37. J. Sun, L. Liu, G. Dong, and J. Zhou, "An extremely broad band metamaterial absorber based on destructive interference," Opt. Express **19**(22), 21155–21162 (2011).
38. K. Chen, R. Adato, and H. Altug, "Dual-band perfect absorber for multispectral plasmon-enhanced infrared spectroscopy," ACS Nano **6**(9), 7998–8006 (2012).
39. B. Zhao, J. Zhao, and Z. Zhang, "Resonance enhanced absorption in a graphene monolayer using deep metal gratings," J. Opt. Soc. Am. B **32**(6), 1176–1185 (2015).
40. N. Nguyen-Huu and Y.-L. Lo, "Tailoring the optical transmission spectra of double-layered compound metallic gratings," IEEE Photonics J. **5**(1), 2700108 (2013).
41. W.-C. Tan, J. R. Sambles, and T. Preist, "Double-period zero-order metal gratings as effective selective absorbers," Phys. Rev. B Condens. Matter Mater. Phys. **61**(19), 13177–13182 (2000).
42. A. P. Hibbins, J. R. Sambles, and C. R. Lawrence, "Excitation of remarkably nondispersive surface plasmons on a nondiffracting, dual-pitch metal grating," Appl. Phys. Lett. **80**(13), 2410–2412 (2002).
43. D. C. Skigin and R. A. Depine, "Diffraction by dual-period gratings," Appl. Opt. **46**(9), 1385–1391 (2007).
44. N. Nguyen-Huu, Y.-L. Lo, Y.-B. Chen, and T.-Y. Yang, "Realization of integrated polarizer and color filters based on subwavelength metallic gratings using a hybrid numerical scheme," Appl. Opt. **50**(4), 415–426 (2011).
45. A. D. Rakić, A. B. Djurišić, J. M. Elazar, and M. L. Majewski, "Optical properties of metallic films for vertical-cavity optoelectronic devices," Appl. Opt. **37**(22), 5271–5283 (1998).
46. A. Vakil and N. Engheta, "Transformation optics using graphene," Science **332**(6035), 1291–1294 (2011).
47. L. Falkovsky, "Optical properties of graphene," J. Phys.: Conf. Ser. **129**, 012004 (2008).
48. D. W. Lynch and W. Hunter, "Comments on the optical constants of metals and an introduction to the data for several metals," in *Handbook of Optical Constants of Solids* (Elsevier, 1997), pp. 275–367.
49. E. D. Palik, *Handbook of Optical Constants of Solids* (Academic Press, 1998).
50. Y. Jiang, S. Pillai, and M. A. Green, "Re-evaluation of literature values of silver optical constants," Opt. Express **23**(3), 2133–2144 (2015).
51. P. B. Johnson and R.-W. Christy, "Optical constants of the noble metals," Phys. Rev. B **6**(12), 4370–4379 (1972).
52. D. Nash and J. Sambles, "Surface plasmon-polariton study of the optical dielectric function of silver," J. Mod. Opt. **43**, 81–91 (1996).
53. H. Miao, A. A. Gomella, N. Chedid, L. Chen, and H. Wen, "Fabrication of 200 nm period hard X-ray phase gratings," Nano Lett. **14**(6), 3453–3458 (2014).
54. Y. Wu, D. Olynick, A. Goodyear, C. Peroz, S. Dhuey, X. Liang, and S. Cabrini, "Cryogenic etching of nano-scale silicon trenches with resist masks," Microelectron. Eng. **88**(8), 2785–2789 (2011).
55. C. Welch, A. Goodyear, T. Wahlbrink, M. C. Lemme, and T. Mollenhauer, "Silicon etch process options for micro-and nanotechnology using inductively coupled plasmas," Microelectron. Eng. **83**(4-9), 1170–1173 (2006).